AAS 24-365

FLIGHT PATH CONTROL ERROR ANALYSIS FOR THE HELIOSWARM OBSERVATORY

Stephen West*, Marissa Intelisano†, Paul Levinson-Muth‡, and Lisa Policastri§

The HelioSwarm Observatory requires specific geometries be formed by the nine satellites in the swarm to resolve different scales of solar wind turbulence. Maneuver execution and state estimation drive flight path control errors that could disrupt the swarm geometry. Using a Monte-Carlo analysis, flight path control errors for dispersed trajectories were generated and the impact to science performance and other mission constraints evaluated. The results highlight the unique aspects of swarm-type multi-satellite missions in terms of maneuver planning and error tolerance.

INTRODUCTION

Multi-point measurements of turbulence in the solar wind can transform our understanding of energy transfer mechanisms from large to fine-scale structures. HelioSwarm is a NASA Medium Explorer (MIDEX) mission that will operate a swarm of nine satellites in a highly eccentric Earth orbit to make the first simultaneous multi-scale solar wind measurements.[1,2] The swarm is composed of a single Hub and eight Node spacecraft. Collectively, the Hub and Nodes are referred to as the Observatory. The Observatory launches with all eight Nodes integrated on the Hub spacecraft. The Hub performs a series of maneuvers to transfer to a highly eccentric 2:1 lunar resonant Earth orbit, referred to herein as P/2 (where P denotes the mean lunar orbit period of 27.3 days). Over the space of several orbits, the eight Nodes separate from the Hub and independently maneuver into carefully selected neighboring orbits. The neighboring orbits produce nearly-periodic relative motion about the Hub. The Nodes perform periodic orbit trim maneuvers (OTMs) to maintain the relative motion. The relative motion of the Nodes about the Hub produces shapes (e.g. tetrahedra) and configurations (e.g. distribution of Nodes along and across the Hub-Sun line). These shapes and configurations enable measurements of solar wind turbulence across multiple scales, revealing the intricacies of energy transfer for the first time. The capability of the Node spacecraft to accurately maintain their assigned relative trajectory, referred to as flight path control, is key to achieving the required Observatory geometries for making these measurements. This paper describes a flight path control error analysis carried out to evaluate the impacts of maneuver execution errors and maneuver planning timeline constraints on the science performance of the HelioSwarm Observatory.

*Sr. Flight Dynamics Engineer, Space Exploration Engineering, 324 Main St. #173, Laurel, MD 20725, stephen@see.com
†Flight Dynamics & Mission Operations Specialist, Space Exploration Engineering, 324 Main St. #173, Laurel, MD 20725, marissa@see.com
‡Aerospace Engineer, NASA Ames Research Center, Moffett Field, CA 94035, paul.g.levinsonmuth@nasa.gov
§Owner & Chief Operating Officer, Space Exploration Engineering, 324 Main St. #173, Laurel, MD 20725, lisa@see.com

The HelioSwarm Observatory

The HelioSwarm Observatory is defined by the coordinated relative motion of eight free-flying Nodes about the Hub spacecraft. The Hub serves as the reference for the swarm since it nominally performs no further translational maneuvers after delivering the eight Nodes to the science orbit. Node relative trajectories are designed in the Hub-centered VNC (velocity-normal-conormal) frame. The VNC y-axis is aligned with the orbit normal (angular momentum vector), the x-axis aligned with the spacecraft velocity vector, and the z-axis completes a right-handed triad. The Node relative trajectories generally fall into three categories: in-plane, out-of-plane, and inner. These categories broadly describe the nature of the Node's relative motion about the Hub. "In-plane" and "out-of-plane" nodes have large amplitude relative motion with maximum ranges on the order of 10^3 km. "Inner" nodes remain in close proximity the Hub with maximum ranges < 250 km. The in-plane Nodes (1, 2, and 5) have relative motion primarily in the Hub-centered velocity-crosstrack (VC) plane. The out-of-plane Nodes (3 and 4) have relative motion primarily in the Hub-centered velocity-normal (VN) plane. The inner Nodes (6, 7, 8) have relative motion in all three axes of the Hub-centered VNC frame. Figure 1 shows two revolutions of the relative trajectory of all eight Nodes in the Hub-centered VNC frame.

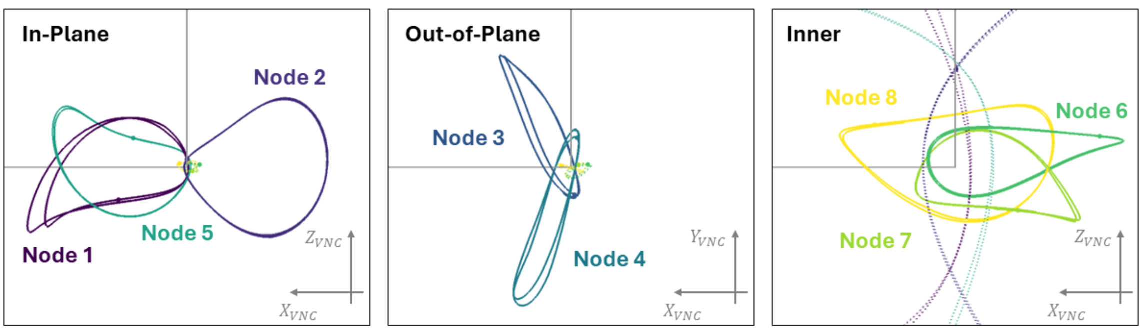

Figure 1. The eight Nodes in the HelioSwarm Observatory generally fall into three categories: in-plane Nodes (l), out-of-plane Nodes (c), and inner Nodes (r). Nominal Node trajectories are shown in the Hub-centered VNC frame. The inner Nodes appear in all three panels as a scale reference.

The HelioSwarm observatory is shaped by geometric configuration requirements that support multi-point, multi-scale turbulence measurement techniques. The first of these configurations requires inter-satellite displacements with short (25-100 km), medium (100-1200 km), and long (> 1200 km) components along all three axes of a reference frame with the x-axis directed along the spacecraft-Sun line, the z-axis aligned with the Sun's spin axis, and the y-axis completing a right-handed triad. This configuration is referred to as the "3D" configuration. The second configuration utilizes common geometric factors describing polyhedra: size (S), elongation (E), and planarity (P).[3] The "Polyhedral" configuration requires that the swarm form two distinct, regular polyhedra with $\sqrt{E^2 + P^2} < 0.6$ and a scale ratio of 3:1. For the purposes of swarm design, the polyhedral configuration is achieved with two polyhedra composed of four spacecraft (tetrahedra). The swarm need not form these polyhedra at a specific point in the orbit. Instead, mission requirements dictate that the Observatory accrue a specified duration of observation time while the swarm satisfies either or both of these configuration requirements. Practically, these swarm design requirements necessitate evaluating each reference swarm design against these requirements to compute the total observation time with the swarm meeting each configuration requirement (3D and Polyhedral).

Node Orbit Trim Maneuvers

Node relative trajectories are carefully selected to be nearly repeating. The P/2 lunar resonant orbit exhibits periodic eccentricity variation of ± 0.05 with a period of $\sim$ 200 days. This eccentricity variation necessitates active control to maintain repeating relative trajectories.[4] Each Node nominally performs two orbit trim maneuvers (OTMs) on each revolution. The ascending OTM occurs between true anomalies $0° \leq \nu < 180°$ while the descending OTM is placed between $180° \leq \nu < 360°$. The ascending and descending OTMs can be shifted within a range of true anomalies for a relatively small Δv penalty.[5] For operational simplicity, the current swarm reference trajectories place the ascending and descending Node OTMs at the same true anomaly for all eight Nodes. Figure 2 shows all Node OTMs for the nominal mission in a polar plot with true anomaly on the tangential axis and maneuver magnitude on the radial axis. Several Nodes have initial maneuvers at different true anomalies as a remnant from the relative trajectory insertion phase which uses a different maneuver strategy (not addressed in this analysis).

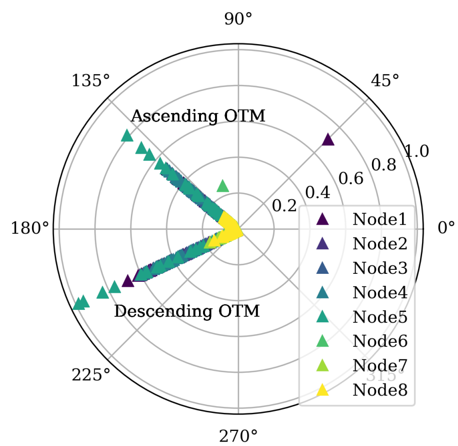

Figure 2. With the exception of initial OTM burns, all Node OTMs occur at fixed values of true anomaly spanning a range of magnitudes up to 1 m/s. OTM magnitude is shown on the radial axis with true anomaly on the tangential axis.

The targeting algorithm for nominal OTMs varies the VNC components of both the ascending and descending OTM on each revolution to achieve target points specified in the Hub VNC frame at given true anomalies. Selection of the target points and OTM placement is part of the overall swarm design process (see Reference 4). Because in-plane and out-of-plane motion is decoupled and the magnitudes of the OTM burns are small, the in-plane and out-of-plane maneuver components can be targeted independently.

The reference swarm trajectory is implemented in Ansys' Systems Tool Kit (STK) using the Astrogator module for targeting and propagation. Both the ascending and descending OTM are targeted on each revolution using a single differential corrector with multiple profiles (each with distinct controls and results). Controls are the VNC components of the ascending and descending OTMs: $\Delta\vec{v} = [\Delta v_x, \Delta v_y, \Delta v_z]$. Results are components of the Node relative position vector in the Hub VNC frame ($\vec{\rho} = [\rho_x, \rho_y, \rho_z]$) evaluated at the target true anomalies (θ_1, θ_2). Tables 1 and 2 show the targeter configurations used to generate the reference swarm trajectories.

Table 1. Targeter configuration for in-plane motion and OTM components

Maneuver	Controls	Segment	Results
Ascending OTM	Δv_x	Propagate to ν_1	ρ_x
	Δv_z		ρ_z
Descending OTM	Δv_z	Propagate to ν_2	ρ_x

Table 2. Targeter configuration for out-of-plane motion and OTM components

Maneuver	Controls	Segment	Results
Ascending OTM	Δv_y	Propagate to ν_1	ρ_y
Descending OTM	Δv_y	Propagate to ν_2	ρ_y

In table 1, $\rho_z(\nu_2)$ (the cornormal component of the relative position vector at the second target point) is omitted from the results. This reflects the reality that the orbit-to-orbit relative trajectory will not be exactly repeating. Allowing some variation in the co-normal direction at the second target true anomaly avoids unnecessary orbit maintenance Δv. To keep the targeting problem well posed (three results, three controls), Δv_x for the descending OTM is omitted.

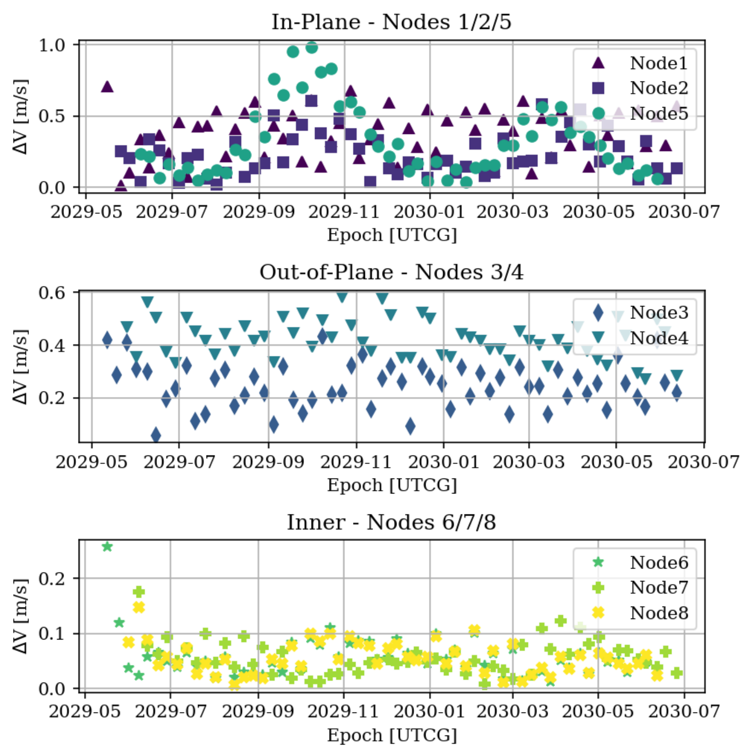

Figure 3. OTM magnitudes fall into three ranges, generally consistent with the three major groupings of Nodes in the Observatory

Figure 3 shows the Δv magnitude for all swarm OTMs over a 14 month nominal mission. This plot does not include the insertion maneuvers required to place the Nodes on their repeating relative trajectories. The amplitude of the relative motion (inner vs. outer Nodes) has a strong influence on the average OTM ΔV with the outer Nodes generally requiring larger OTM magnitudes than the inner Nodes. Some Nodes exhibit a seasonal variation in OTM magnitude that can be attributed to the periodic variation in the science orbit eccentricity.

Since OTMs are required to maintain the reference swarm trajectories, these maneuvers are deterministic. However, OTMs must also correct for execution errors in previous maneuvers and, as a result, have a statistical component that is not reflected in these nominal values. Additionally, some of the OTM magnitudes, particularly for the inner Nodes, are small enough that they would likely be waived in operations. For the purposes of this study, no minimum maneuver magnitude is enforced and no OTMs are waived. These perturbations from the nominal OTM values drive flight path control error between the reference and actual Node trajectories. Flight path control describes the degree to which a maneuverable spacecraft can follow a proscribed reference trajectory under the influence of expected uncertainties, errors, and perturbations. Flight path control analysis verifies that trajectory requirements are met with expected performance from spacecraft systems (e.g. propulsion, attitude control) and the mission ground segment (e.g. navigation, maneuver planning)

Swarm Management Considerations

As a small satellite swarm, the HelioSwarm Observatory is distinct from other types of multi-satellite mission architectures both in the scale of the relative trajectories (2-3 orders of magnitude smaller than the absolute inertial orbit scale) and in the criticality of maintenance maneuvers. The small satellite swarm architecture offers a cost-effective means of implementing nine satellites operating as a collective entity. The swarm concept embraces the idea that no single maneuver is critical, where failing to perform the maneuver would lead to an immediate contingency situation (e.g. recontact or loss of spacecraft due to exceeding inter-satellite communications range). This philosophy also eases requirements on the precision of maneuver planning and execution, relaxing expectations for ground operations turn-around time (measurement downlink to maneuver command uplink) and accepting maneuver performance capabilities of extant small satellite propulsion systems.

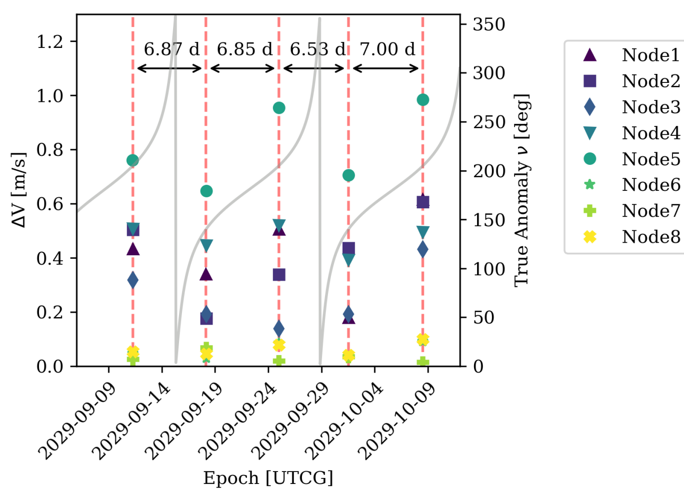

Figure 4. Ascending and descending OTMs occur every 6-7 days with the exact duration between maneuvers varying with the orbit period

As a multi-satellite mission in highly eccentric orbit, HelioSwarm has unique challenges in terms of flight dynamics operations. The timescale of relative motion in the P/2 orbit is $\sim$ 13.7 days.

With two maneuvers per revolution, the maneuver cadence is one maneuver every 6-7 days. Since the nominal maneuvers are fixed in true anomaly, the cadence varies throughout the mission as the eccentricity varies. Figure 4 shows 2.5 revolutions early in the nominal mission with maneuver placement shown both in time and orbit true anomaly.

HelioSwarm flight dynamics operations include orbit determination, maneuver estimation, and maneuver planning. HelioSwarm leverages high-heritage ground systems and processes to perform all flight dynamics operations, avoiding the cost of developing and verifying new on-board capabilities. Performing orbit determination and maneuver estimation for spacecraft in cislunar, multi-day period orbits is challenging due to the extended timescales of motion and the resultant slow variation of measurement observables (e.g. range). Post-maneuver orbit estimates can require a significant portion of the orbit to converge.[6,7] With two maneuvers per orbit, it may not be possible to complete maneuver estimation of the previous OTM prior to planning the upcoming OTM. The robustness of the swarm architecture should gracefully tolerate flight path control errors introduced due to maneuver planning timeline constraints, but this must be verified by analysis against the science performance requirements.

MANEUVER ESTIMATION

Previous orbit determination error analyses for HelioSwarm have been performed using Ansys' Orbit Determination Tool Kit (ODTK).[8] This analysis is expanded to included maneuver estimation in the presence of unknown execution errors. The error in the estimated maneuver is trended over a full revolution of daily post-maneuver ranging sessions to determine the time required to converge the statistical maneuver estimate.

Node Orbit Determination

HelioSwarm's Hub spacecraft is tracked by Earth ground stations generating radiometric range and range rate measurements used for orbit determination. For this analysis, the ground network was assumed to be NASA's Deep Space Network (DSN). Specifically, simulated sequential range and total count phase (TCP) measurements are generated with measurement characteristics representative of the 34 meter beam waveguide antennae in Goldstone, CA, USA (DSS24); Canberra, Australia (DSS34); and Madrid, Spain (DSS54).

The Node spacecraft communicate with ground exclusively through the Hub spacecraft using a hub-and-spoke network topology. The space communication system (SCS) generates radiometric range measurements between the Hub and Node spacecraft. Simulated space-based range measurements are generated with measurement characteristics representative of notional SCS performance.

The Node spacecraft each simulate one 30-minute ranging session with the Hub every day as a part of nominal swarm operations. The Hub simulates four tracking passes with the ground network throughout each revolution in the science orbit. For this analysis, nominal tracking passes were placed at Hub true anomalies of 90°, 150°, 210°, and 270°. A simplistic scheduling algorithm alternates between the three DSN stations and chose view periods closest to the desired true anomaly. Figure 5 shows a representative tracking schedule for Node 3 and the Hub. The "RangingInst" tracker represents the Hub-mounted SCS transceiver generating the relative ranging measurement.

Simulated measurements are processed using ODTK's optimal sequential filter to generate a definitive ephemeris. A reverse smoother is then used to eliminate discontinuities in the filter

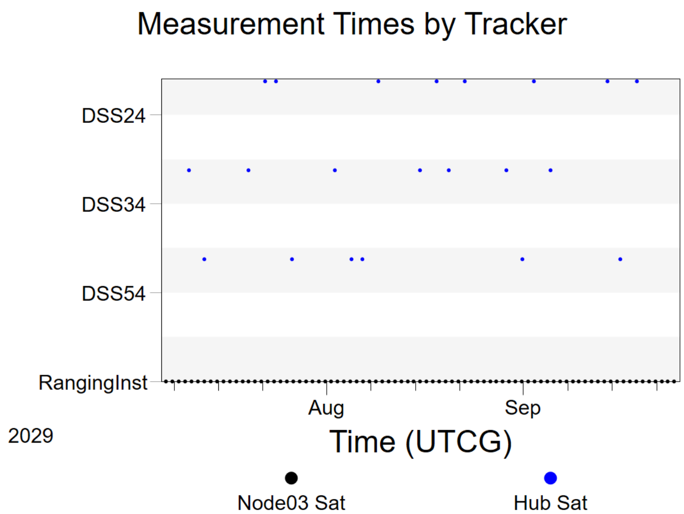

Figure 5. Simulated tracking schedule includes DSS24, DSS34, and DSS54 for the Hub along with daily 30-minute space-based ranging sessions between the Hub and each Node. Example measurements for Node 3 are shown grouped by tracker.

ephemeris and reduce the uncertainty of the definitive orbit estimate by incorporating future knowledge of the estimated state.[8] The combined filter-smoother process also generates estimates of modeled maneuvers.

This analysis focuses on maneuver estimation performance during nominal swarm operations. At this stage in the mission, the tracking system (including the ground network and SCS) is assumed to be calibrated, maneuvers recovered to within 0.1% and $0.1°$ of the actual maneuver, and the filter properly tuned for the nominal trajectory and tracking schedule. To simulate this, the filter is run for several revolutions in order to reach steady state. The actual values of maneuvers modeled in the simulated data are included in the filter spacecraft dynamics model (consistent with successful and accurate estimation of prior maneuvers). Figure 6 shows the residual ratios (measurement residual divided by measurement root error variance) for Node 3 and the Hub as an example of a well tuned, steady state filter accepting simulated measurements from both the DSN and the Hub SCS.

In steady state, the uncertainty should not exhibit large secular variation. Figure 7 shows the 3σ filter position uncertainty for Node 3 and the Hub. The first few days of the filter run show a large transient as the initial orbit uncertainty collapses. This is an artifact of initializing a filter run for OD error analysis using simulated data at an arbitrary point mid-mission. In operations, each Node's orbit estimate will be initialized from the existing Hub orbit estimate which is continuous from launch vehicle separation. This study focuses on Node maneuver estimation (since the Hub performs no translational maneuvers during the science phase) and does not address the orbit estimation during the Hub's (with all eight Nodes attached) transfer from launch to the science orbit. Figure 7 does not exhibit any large transients after the first several days indicating that the filter has reached steady state.

Steady state filter behavior can further be confirmed by examining the smoothed position uncertainty, shown in figure 8. The smoothed position uncertainty shows periodic variation consistent with the orbit period but has no secular trend.

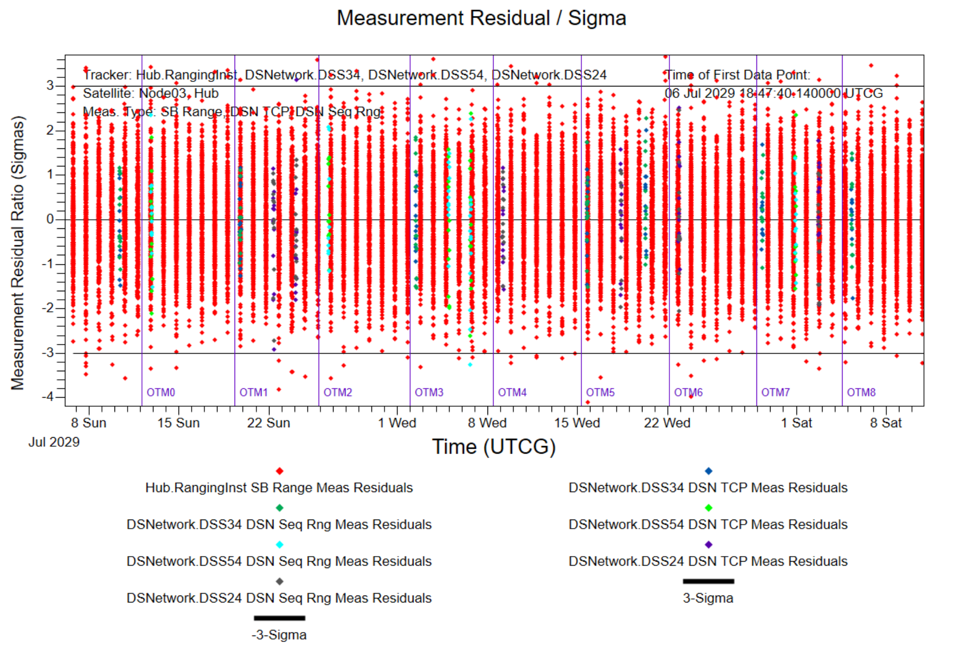

Figure 6. Steady state filter accepts and processes nearly all simulated measurements from ground network and Hub SCS indicating proper tuning

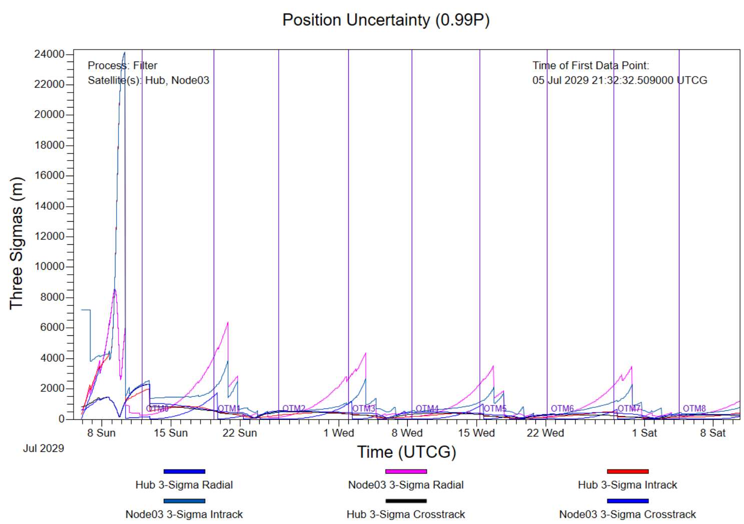

Figure 7. Filter position uncertainty (3σ) reaches steady state after a transient during which the initial orbit uncertainty collapses. Small periodic uncertainty increases correspond approximately with the orbit period.

Convergence Study

To evaluate the convergence behavior of maneuver estimates, a final OTM is included in the simulated measurement data. Maneuver execution error is simulated by perturbing the maneuver parameters specified in the filter spacecraft dynamics model. In operations, orbit determination must use the planned value of spacecraft maneuvers to estimate the errors on the as-flown maneuver. This

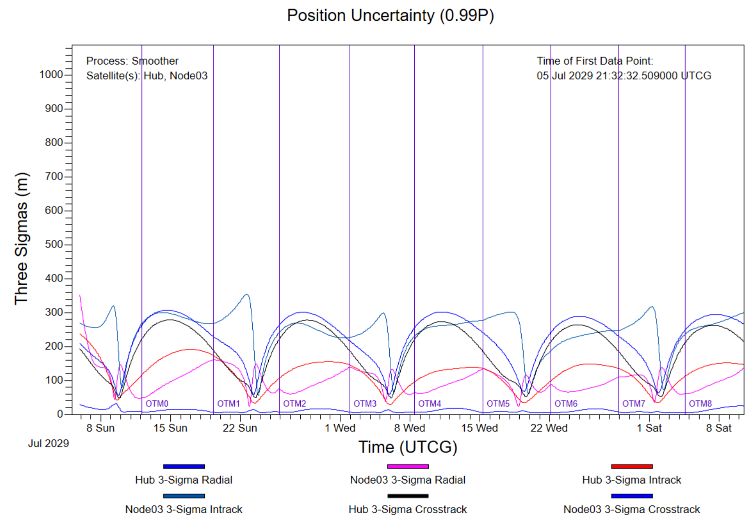

Figure 8. Smoothed position uncertainty (3σ) shows steady state orbit estimate with periodic variation in the position uncertainty corresponding to the orbit period and no secular trend.

study avoids additional measurement simulation by applying this uncertainty to the filter dynamics model rather than the measurement simulation. The convergence behavior is observed by running the filter/smoother process after each daily space-based ranging pass for just over one complete revolution after the perturbed maneuver (14 passes). While this is inconsistent with the HelioSwarm operational concept's two maneuvers per orbit, isolating the perturbed maneuver eliminates other factors (e.g. a subsequent OTM) that could obscure the convergence behavior of the maneuver estimate. The goal for this study is to evaluate the convergence behavior of the maneuver estimates rather than model the specific HelioSwarm concept of operations.

In addition to the predicted maneuver values, the uncertainty in the maneuver magnitude and pointing is also specified in the filter dynamics model. Since both the actual and perturbed maneuver values are known in this study, the filter maneuver uncertainty parameters can be configured to represent a 1σ, 2σ, or 3σ error. The results of this convergence study reveal the time required to estimate each maneuver in the Node trajectory.

Slow relative motion relative to the Hub at apogee as compared to faster relative motion near perigee suggests that the descending and ascending OTMs may have different maneuver estimation convergence behavior. As such, representative ascending and descending OTMs for Nodes 1-4 were processed using the method described above. A consistent 5%, 5° perturbation was applied to each maneuver. To model this perturbation as a 1σ, 2σ, or 3σ error, the filter was configured with a 5%, 5°; 2.5%, 2.5°; or 1.67%, 1.67° uncertainty, respectively. For some Nodes, modeling the 5%, 5° perturbation as a 3σ error (1.67%, 1.67° uncertainty) led to measurements being rejected and the filter failing to re-converge after the maneuver. Operationally, this signature cues the analyst to increase the uncertainty of the maneuver in the filter dynamics model. In this study, scenarios where the input filter uncertainty led to non-convergence were omitted from the results.

Maneuver Recovery Timeline

Figure 9 shows the results of the convergence study. The error between the estimated and actual maneuver is evaluated after each of the 14 post-maneuver relative ranging sessions. Convergence is indicated when both magnitude and pointing approach the horizontal axis (zero error). Magnitude errors are shown with solid lines and diamonds, pointing errors with dashed lines and circles. The descending maneuvers show a consistent trend towards convergence around 6-7 days post-maneuver. The ascending maneuvers are less consistent Node-to-Node but generally require longer durations to reach steady state.

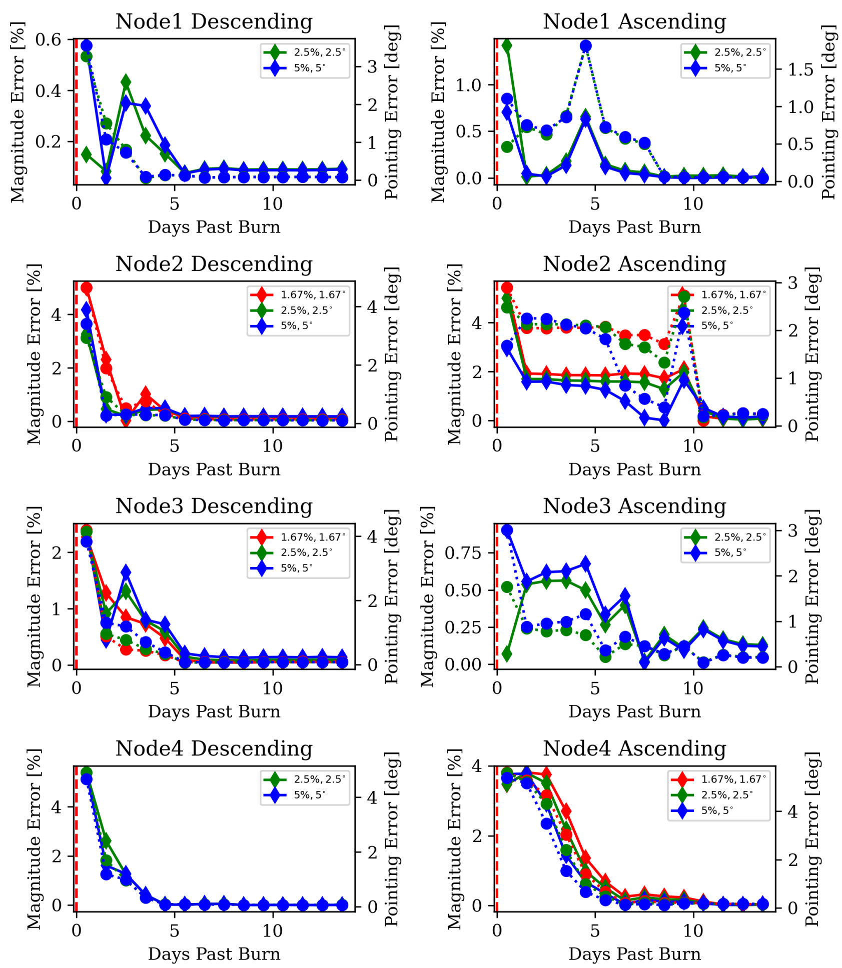

Figure 9. Descending maneuver estimation reaches steady state after 6-7 days while ascending maneuvers reach steady state on longer timelines

This study focused on Nodes 1-4 since the similarity in their maneuver magnitudes enabled a direct comparison using the same process and filter configurations for all four Nodes. The inner Nodes exhibited similar behaviors, but the small size of inner Node OTMs required tailoring the filter dynamic model maneuver uncertainty precluding a direct comparison. Node 5 also required tailoring of the filter maneuver uncertainty parameters due to the large variation in the magnitudes of Node 5 OTMs. While this tailoring is standard in an operational context, this study applied identical filter settings to a variety of Nodes, precluding the use of Nodes 5-8. Since the timescale of motion in the P/2 orbit is the driving factor behind the maneuver estimation convergence behavior, the same trends (requiring over half a revolution to converge) are expected to apply to Nodes 5-8.

These results clearly indicate that recovering a maneuver in high altitude, highly eccentric Earth orbits requires measurements over a substantial arc of the orbit. For HelioSwarm's two-maneuver-per-orbit cadence, this indicates that it may not be possible to complete maneuver estimation and establish a new orbit estimate after an OTM in sufficient time to plan, sequence, and command the subsequent OTM. The impact of this operational timeline is that OTMs may be planned with outdated state information, introducing an additional source of error. The swarm concept is intended to be robust against maneuver execution errors, but the science performance of the HelioSwarm Observatory must be verified in the presence of these errors.

FLIGHT PATH CONTROL ERROR ANALYSIS

A flight path control error analysis is carried out to evaluate the impacts of maneuver execution errors and maneuver planning timeline constraints on the science performance of the HelioSwarm Observatory. Each Node's flight path control is independent of the other Nodes in the swarm. Orbit determination for each Node relies on Hub-Node range measurement (in addition the ground-based tracking measurements of the Hub). Maneuver planning for each Node drives the trajectory to fixed Cartesian target points at specific true anomalies. Since each Node is independent of the others, dispersed trajectories can be generated for each Node and combined to evaluate the science performance of the Observatory.

Node Flight Path Dispersion

Node flight path errors stem from three sources:

State estimation errors: Maneuver planning uses the estimated Node state. Assuming the covariance is realistic (a separate analysis and tuning process), the error between the actual and estimated state is represented by the covariance associated with the Node state estimate. This error results in a slightly different maneuver being planned than the maneuver that would result from perfect state knowledge. A key consideration for determining state estimation errors applicable for maneuver planning is the maneuver planning timeline. Typical maneuver planning processes include a data cutoff (DCO) epoch that represents the last opportunity to incorporate new measurements into the state estimate used for maneuver planning. The estimated state and associated covariance must be propagated to the maneuver epoch to understand the potential errors in state estimation relevant to maneuver execution. Generally, the greater duration between DCO and maneuver execution, the greater the significance of state estimation errors. For HelioSwarm, the results presented above suggest that maneuver estimates may not converge prior to the planning process for the subsequent maneuver. As a result, the state estimate used for planning any give OTM may have to be pulled from an epoch prior to the previous OTM. This is an additional factor contributing to state estimation error.

Initial state errors: Propagation of errors and dispersions from prior mission phases results in an offset between the actual and desired initial state. For the nominal Node operations during science phase, initial state errors stem from the Hub orbit insertion errors, dispersions on the Node separation from the Hub, and flight path control errors prior to achieving the desired relative trajectories.

Maneuver execution errors: Intricacies of spacecraft propulsion systems (e.g. tank pressures, valve response times, thruster performance variability) produce errors between the commanded and executed maneuver magnitude. Thrust vector control during a propulsive maneuver also has attendant dispersion and errors resulting in error between the commanded and executed maneuver direction. These errors combined result in a perturbation to the post-maneuver orbit. The HelioSwarm

Nodes use small satellite propulsion systems which may contribute to larger maneuver execution errors than legacy propulsion systems for larger satellites with greater flight heritage to characterize performance.

Method

The Node flight path control analysis uses a Monte Carlo method to apply initial state, state estimation, and maneuver execution error to Node trajectory simulations. For this analysis, the maneuver planning timeline constraint and expected maneuver execution errors are the primary consideration with other error sources omitted. An STK scenario is configured to model both the planning and execution of both ascending and descending OTMs. Given the challenge with recovering either OTM within the 6-7 days planning window, it is assumed each OTM must be planned using the estimated state prior to the previous maneuver. The Node trajectory is propagated through the prior maneuver, assuming nominal maneuver values, up to the epoch of the OTM being planned. Figure 10 shows this maneuver planning concept. Planning OTM-n uses the Node estimated state immediately prior to OTM-(n-1). In effect, the maneuver planning processes for a given OTM ”leapfrogs” the previous maneuver.

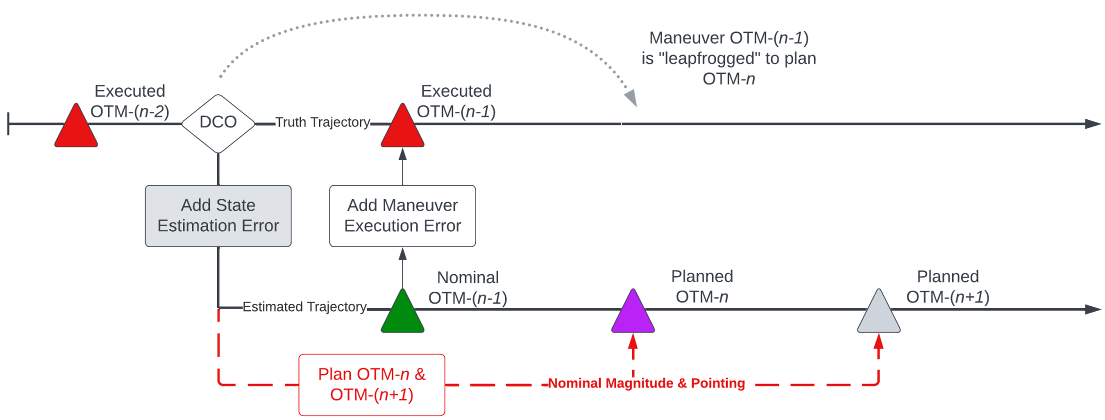

Figure 10. Flight path control error analysis simulates planning OTM-n using a state pulled prior to OTM-(n-1), consistent with the planning timelines for two maneuvers per revolution in a P/2 lunar resonant orbit

Figure 10 shows two subsequent OTMs, OTM-n and OTM-(n+1). Two OTMs are required to keep the targeting algorithm well-posed. Targeting the ascending OTM uses the nominal swarm design OTM targeting algorithm shown in tables 1 and 2. The descending OTM requires a similar targeting algorithm that includes the ascending OTM from the next revolution. Tables 3 and 4 show the modifications made to the targeting algorithm for the descending OTM. As in the nominal swarm design OTM targeting algorithm, the VNC-z component of the target point at ν_1 is left unconstrained to accommodate relative trajectory variations due to science orbit eccentricity. Additionally, an additional OTM velocity component is included, making the in-plane targeter slightly under-constrained. This is required to accommodate dispersions on the prior ascending OTM.

In order to isolate the maneuver planning timeline constraint, no additional state estimation error is applied to the state sampled prior to the previous OTM. This assumes that the prolonged propa-

Table 3. Targeter configuration for in-plane motion and descending OTM components

Maneuver	Controls	Segment	Results
Descending OTM	Δv_x	Propagate to ν_2	ρ_z
	Δv_z		ρ_x
Ascending OTM (next rev)	Δv_x	Propagate to ν_1 (next rev)	ρ_x
	Δv_z		

Table 4. Targeter configuration for out-of-plane motion and descending OTM components

Maneuver	Controls	Segment	Results
Descending OTM	Δv_y	Propagate to ν_2	ρ_y
Ascending OTM (next rev)	Δv_y	Propagate to ν_1 (next rev)	ρ_y

gation including a nominal (as opposed to executed) maneuver will be a larger error source than the state estimation error. Additionally, this simplification isolates the impact of the maneuver planning timeline constraint.

Each Monte-Carlo simulation includes 100 iterations. Three scenarios for maneuver execution error were run: 5% magnitude error with 5° pointing error, 5% magnitude error only, and 5° pointing error only. Errors are specified at the 3σ level. Observatory science performance is evaluated with all Nodes dispersed. For comparison, Observatory science performance is also evaluated with only a single group of Nodes (inner, in-plane, out-of-plane) dispersed and the other 5-6 Nodes following nominal trajectories. This comparison reveals which Nodes' contribution to science performance is most adversely impacted by flight path control errors.

Dispersed Trajectories

Comparison of flight path control errors resulting from applied maneuver dispersions requires a scalar quantity. The scalar flight path control error (ϵ) is defined in Equation 1 as the root-sum-square of the difference (at each instance in time) between the dispersed ($\vec{\rho}$) and nominal ($\vec{r}$) trajectory.

$$\epsilon = \sqrt{(\rho_x - r_x)^2 + (\rho_y - r_y)^2 + (\rho_z - r_z)^2} \tag{1}$$

Figure 11 shows the flight path control errors for all eight Nodes subject to magnitude-only, pointing-only, and combined magnitude and pointing errors. In Figure 11, the solid line shows the mean value for flight path control error (across 100 iterations) while the shaded region spans from the minimum to the maximum flight path control error. Shaded regions are drawn with transparency such that areas of overlap (between different datasets) are indicated by the complementary colors (e.g. purple region is the overlap of red and blue regions). True anomaly (from the nominal trajectory) is shown on the secondary y-axis as a reference.

From Figure 11, it is evident that direction dispersions have a much more significant impact on the flight path control error than magnitude dispersions. This is indicated both by low values of the mean magnitude-only flight path control error and by the similarity of the direction-only and magnitude-and-direction errors. Given this result, the magnitude and direction dispersion can be considered the stressing case. Dispersed trajectory results for the case of both magnitude and direction dispersion

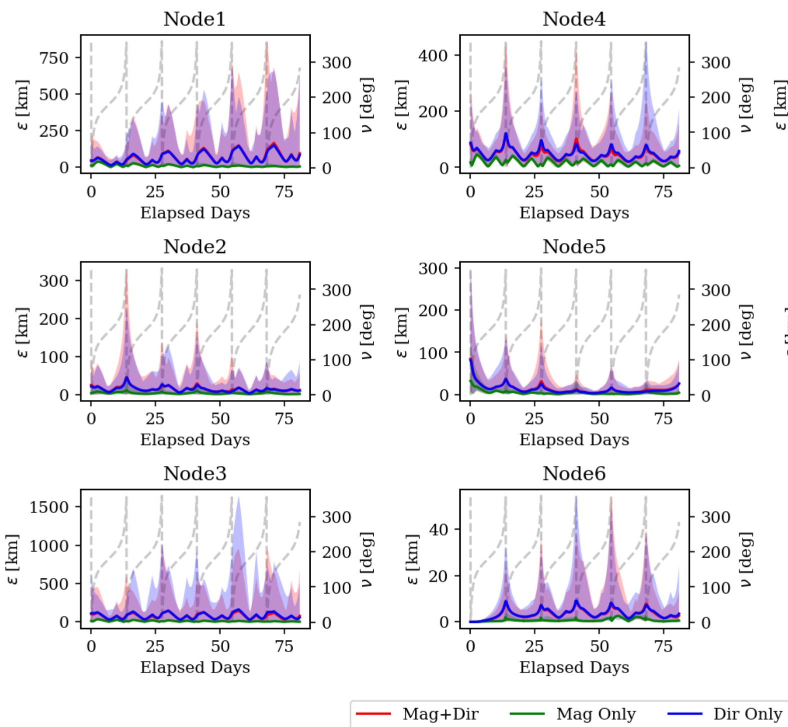

Figure 11. Flight path control errors for Nodes 1-8 with maneuver planning timeline constraints and applied perturbations in maneuver magnitude, direction, and both magnitude and direction.

illustrate the qualitative nature of dispersed Node trajectories. Figure 12 shows dispersed trajectories for all eight Nodes projected into the Hub-centered velocity-conormal plane to illustrate the relative flight path deviations. The nominal trajectory is shown in black with the dispersed trajectories overlaid in color. In Figure 12, Nodes 1 and 3 exhibit a higher degree of deviation from the reference trajectory. Given similarities with other Nodes (e.d. Node 1 and Node 5 similarity, Node 3 and Node 4 similarity), this suggests that the particulars of the nominal OTM targeting algorithm for Nodes 1 and 3 increases its sensitivity to maneuver execution errors. This result is expected given the application of the nominal OTM targeting algorithm to a dispersed trajectory. Nodes exhibiting unwanted sensitivity are candidates for implementing a more operationally-representative OTM targeting algorithm that is robust against these dispersions. Figure 13 shows the Hub-Node range for the Nodes with nominal range shown in black and dispersed ranges shown in color. Finally, Figure 15 shows a histogram of the total ΔV for each iteration with the nominal and 95th percentile ΔV ("DV95") indicated by the black and red lines respectively. DV95 was computed from a kernel density estimate (KDE) using Scott bandwidth estimation shown by the solid line in Figure 15. Figure 14 shows a histogram of the minimum Hub-Node range for each iteration of the Node flight path control error study. The nominal minimum range is shown with the black dashed line.

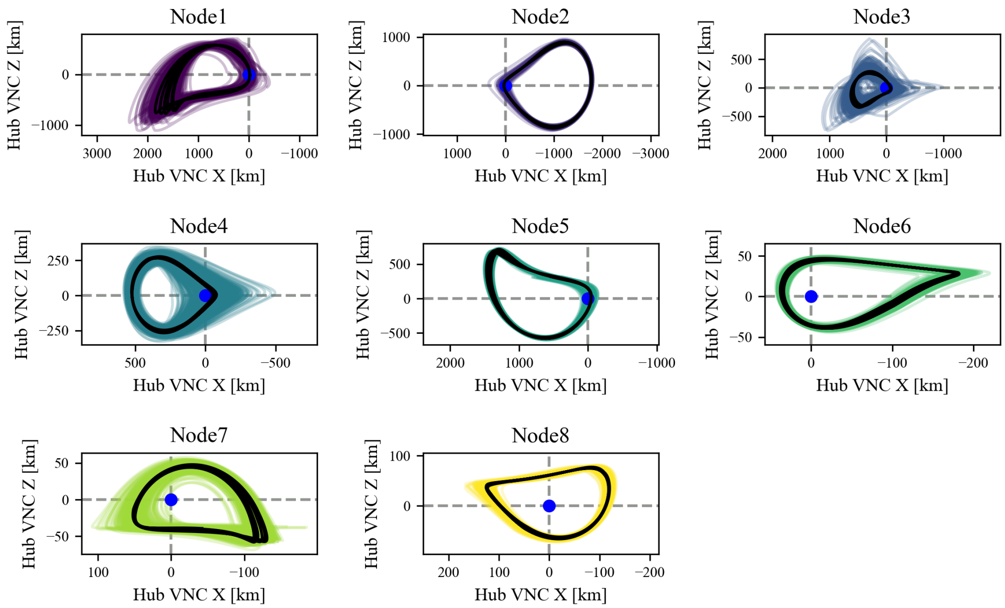

Figure 12. Dispersed (color) and nominal (black) Node trajectories for 100 Monte-Carlo iterations with maneuver execution error and maneuver planning timeline constraints projected into the Hub velocity-conormal plane.

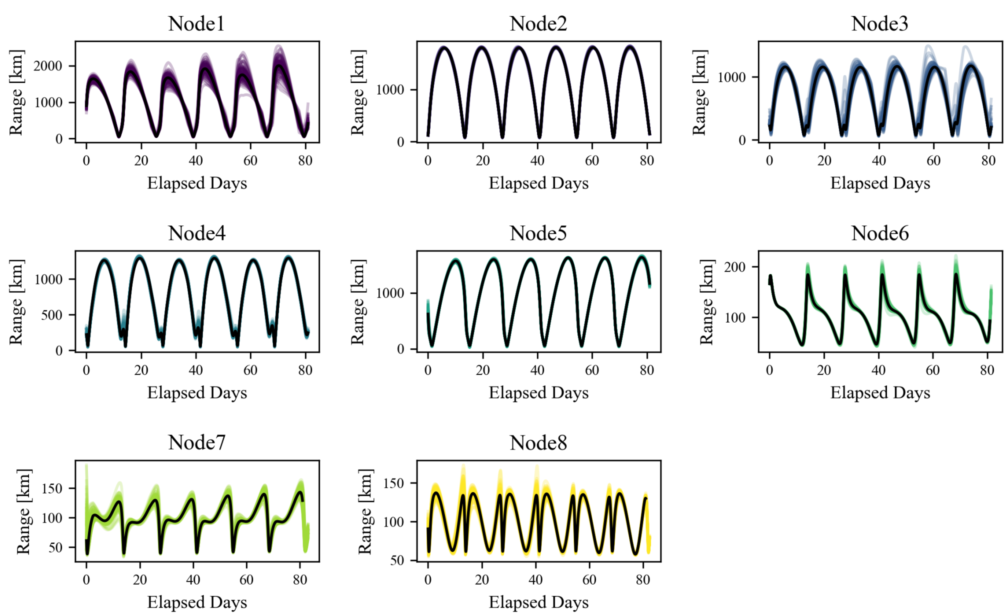

Figure 13. Dispersed Hub-Node ranges for 100 Monte-Carlo iterations with maneuver execution error and maneuver planning timeline constraints. Nominal range is shown in black with dispersed ranges shown in color.

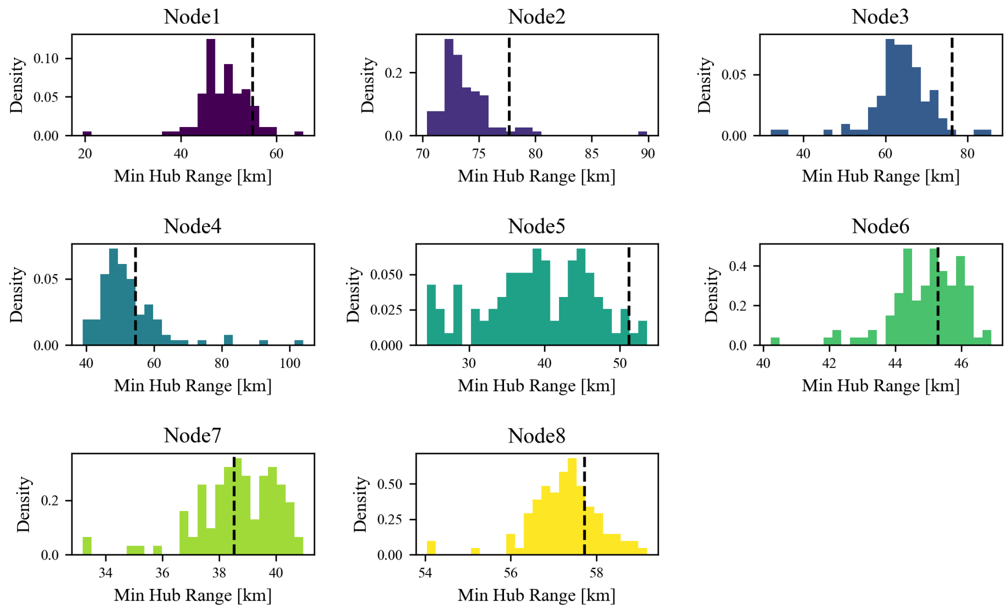

Figure 14. Minimum Hub-Node range for 100 Monte-Carlo iterations with maneuver execution error and maneuver planning timeline constraints.

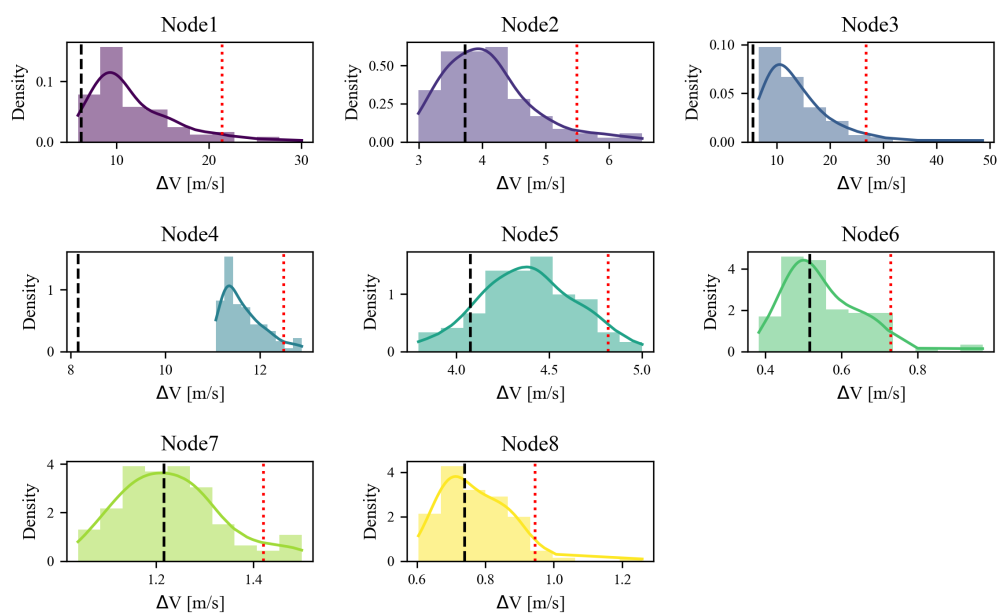

Figure 15. ΔV for 100 Monte-Carlo iterations with maneuver execution error and maneuver planning timeline constraints. Black dashed line indicates DRM ΔV, red dotted line indicates 95th percentile ΔV computed from kernel density estimate using Scott bandwith estimation.

Observatory Science Performance

The science performance of the HelioSwarm Observatory is evaluated by computing the number of one-hour increments accrued in each of the Observatory geometric configurations ("3D" and

“Polyhedral”). Hours are divided between periods where the entire Observatory is in the pristine solar wind (PSW), beyond the influence of Earth’s magnetosphere, and periods where the Observatory is within the magnetosphere, exposed to strongly driven (SD) turbulence. Table 5 summarizes the science performance for twelve scenarios. Dispersions are applied to all Nodes and each group of Nodes (inner, in-plane, out-of-plane) with other Nodes following nominal trajectories. Maneuver execution errors are applied to maneuver magnitude, direction, and both magnitude and direction. Since the simulation only covers a small portion (6 of 26 total orbit revolutions) of the science phase, these Observatory performance metrics represent the relative impact of the dispersed inner Node trajectories. Figure 16 shows histograms of the total hour increments accrued in each region with all Nodes perturbed. The magnitude and direction, magnitude only, and direction only datasets are colored red, green, and blue, respectively. As in Figure 11, colored regions for each dataset are drawn with transparency such that regions of overlap can be observed by the mixing of primary colors (e.g. purple region is the overlap between red and blue). Figure 17 shows the time-history of science hour accrual. The black line indicates the number of science observation intervals accrued at each instant in time. The colored regions span from the minimum to the maximum number of science observation intervals accrued at that instant across the 100 Monte-Carlo iterations. The red dashed line in Figure 17 indicates the required number of hours in each region.

The Observatory satisfies three out of four science observation requirements over just the first six out of 26 revolutions in the science orbit. The introduction of maneuver execution and the maneuver planning constraint (“leap-frogging”) causes some variation int the total number of science hours accrued. For all 100 dispersed trajectories, the three science observation requirements met by the reference (nominal) trajectory are still satisfied.

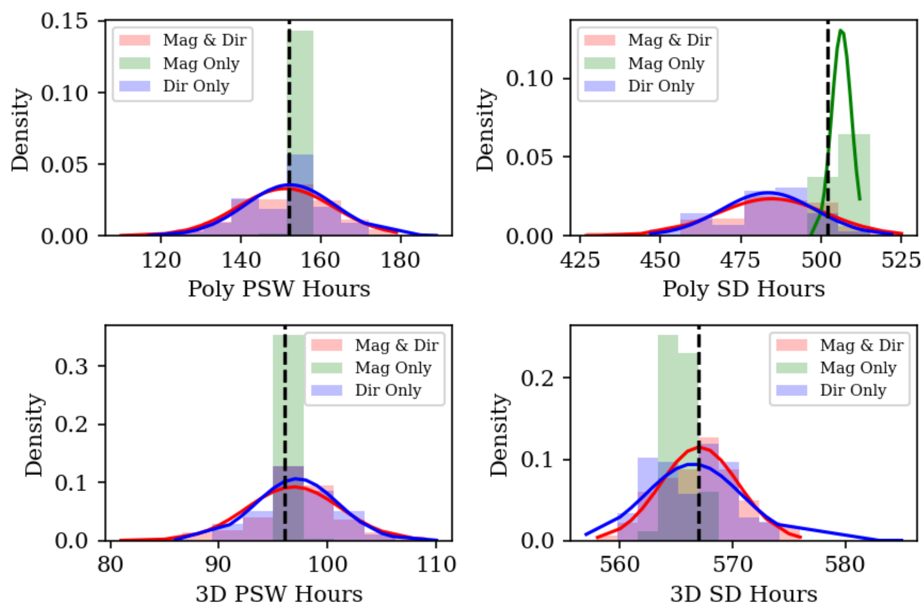

Figure 16. Histogram of science observation hours accrued in each region of interest. Shaded regions show distributions for dispersions applied to maneuver magnitude, maneuver direction, and both magnitude and direction. Solid lines show normal fits to each distribution.

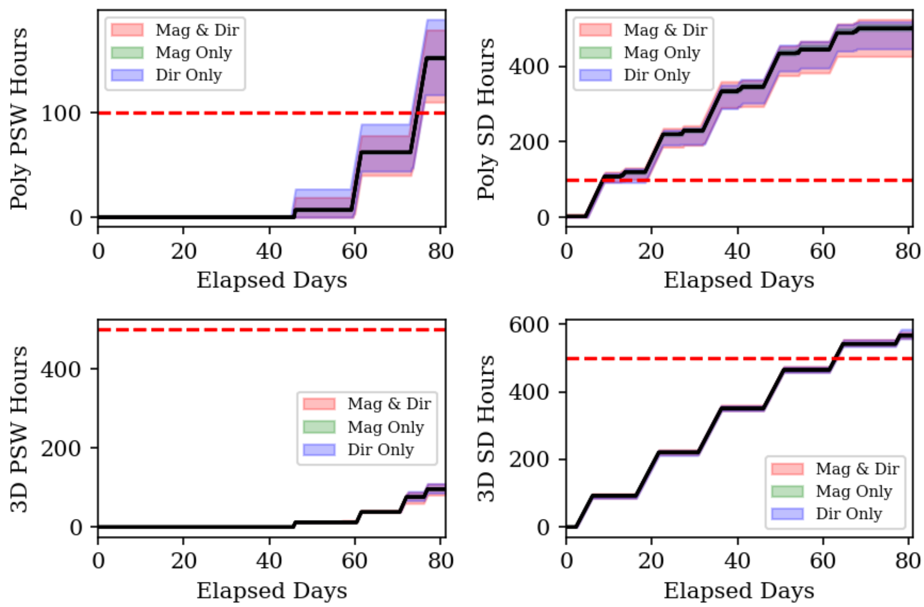

Figure 17. Time history of science observation hours accrued over six revolutions in science orbit. Solid line show nominal Observatory. Shaded regions span from minimum to maximum science hours at each time instance for dispersed Observatory. The mission science requirement levied on each science observation metric is marked with a dashed red line.

Discussion

The maneuver estimation convergence study indicates that multiple days are required to accurately estimate small orbit trim maneuvers in high altitude, highly eccentric lunar resonant orbit. Given HelioSwarm's two maneuver per orbit cadence, this timeline requires maneuvers to be planned without knowledge of the previous maneuver outcome. Effectively, this requires planning OTM-n with a state estimate taken prior to OTM-(n-1). The state used to plan OTM-n includes nominal parameters for OTM-(n-1) and does not account for maneuver execution errors on the previous burn. This error source manifests as a state estimation dispersion and drives a flight path control error for the Node spacecraft. The impact of this error is evaluated by simulating a perturbed swarm subject to maneuver execution errors and maneuver planning timeline constraints. Table 5 shows that the flight path error introduced by these error source causes less than a 5% variation in accrued science hours as compared to the nominal, unperturbed swarm. This is consistent with the qualitative results showing limited deviation from the nominal trajectories.

This behavior for the swarm is expected and consistent with the design philosophy for the HelioSwarm Observatory. By leveraging natural motion and only relying on OTMs to manage orbit perturbations, the Observatory geometry is relatively insensitive to maneuver errors. As a result, the science performance is not compromised even subject to less-than-ideal maneuver planning constraints. Both of these attributes are key to operating a nine-spacecraft Observatory within the limits imposed by the MIDEX mission cost cap.

Conclusion

The HelioSwarm Observatory requires specific swarm geometric configurations be achieved and maintained to accrue sufficient observation hours to meet science requirements. The slow timescale of motion in a highly eccentric lunar resonant orbit and relatively frequent maneuver cadence (twice per revolution) during nominal operations require maneuvers to be planned without a statistical estimate of the prior maneuver outcome. This maneuver planning constraint in combination with maneuver execution errors drives flight path control errors for the Nodes. The swarm architecture is robust to these errors with science performance metrics degrading by less than 5% in the presence of these errors. These results illustrate the advantage of swarm architectures for performing multi-satellite observations in an operationally constrained environment.

REFERENCES

[1] K. G. Klein, H. Spence, O. Alexandrova, M. Argall, L. Arzamasskiy, J. Bookbinder, T. Broeren, D. Caprioli, A. Case, B. Chandran, L.-J. Chen, I. Dors, J. Eastwood, C. Forsyth, A. Galvin, V. Genot, J. Halekas, M. Hesse, B. Hine, T. Horbury, L. Jian, J. Kasper, M. Kretzschmar, M. Kunz, B. Lavraud, O. Le Contel, A. Mallet, B. Maruca, W. Matthaeus, J. Niehof, H. O'Brien, C. Owen, A. Retinò, C. Reynolds, O. Roberts, A. Schekochihin, R. Skoug, C. Smith, S. Smith, J. Steinberg, M. Stevens, A. Szabo, J. TenBarge, R. Torbert, B. Vasquez, D. Verscharen, P. Whittlesey, B. Wickizer, G. Zank, and E. Zweibel, "HelioSwarm: A Multipoint, Multiscale Mission to Characterize Turbulence," *Space Science Reviews*, Vol. 219, Nov 2023, p. 74, 10.1007/s11214-023-01019-0.

[2] L. Plice, A. Dono Perez, and S. West, "HelioSwarm: swarm mission design in high altitude orbit for heliophysics," *AAS/AIAA Astrodynamics Specialist Conference*, Portland, ME, 2019.

[3] P. Robert, A. Roux, C. Harvey, M. Dunlop, P. Daly, and K.-H. Glassmeir, "Tetrahedron Geometric Factors," *Analysis Methods for Multi-Sapcecraft Data* (G. Paschmann and P. W. Daly, eds.), Noordwijk, The Netherlands: ESA Publications Division, 1998.

[4] P. Levinson-Muth, S. West, and L. Plice, "HelioSwarm: swarm design methods in eccentric P/2 lunar resonant orbit," *AAS/AIAA Astrodynamics Specialist Conferece*, Charlotte, NC, 2022.

[5] P. Levinson-Muth, L. Plice, and J. Alvarellos, "HelioSwarm: relative orbit maintenance in eccentric P/2 lunar resonant orbit," *AAS/AIAA Astrodynamics Specialist Conference*, Virtual, 2021.

[6] L. Policastri, J. Carrico, T. Craychee, T. Johnson, and J. Woodburn, "Orbit determination operations for the interstellar boundary explorer," *AAS/AIAA Spaceflight Mechanics Meeting*, Savannah, GA, 2009.

[7] R. Lebois, L. Policastri, J. Carrico, and M. Intelisano, "Extended mission maneuver operations for the interstellar boundar explorer (IBEX)," *AAS/AIAA Spaceflight Mechanics Meeting*, Charleston, SC, 2012.

[8] L. Policastri and J. Woodburn, "HelioSwarm: space-based relative ranging for cubesat cluster mission in a 2:1 lunar resonant orbit," *AAS/AIAA Astrodynamics Specialist Conference*, Portland, ME, 2019.

Table 5. Observatory science performance statistics for 100 iterations with inner Nodes dispersed, outer Nodes nominal. The first row shows results from the DRM with no perturbations. Subsequent rows summarize perturbed Observatory performance in absolute and relative terms.

Metric	DRM	[i] Perturb Node 1/2/5				[ii] Perturb Node 3/4				[iii] Perturb Node 6/7/8				[iv] Perturb All Nodes			
(a) Magnitude & Direction																	
		Min	*Max*	*Mean*	σ	*Min*	*Max*	*Mean*	σ	*Min*	*Max*	*Mean*	σ	*Min*	*Max*	*Mean*	σ
PSW-3D	99	86	111	99	3.80	92	107	99	2.00	99	99	99	0.00	81	109	97	4.32
SD-3D	556	551	567	557	2.65	550	564	555	2.59	529	564	555	9.8	5578	576	567	3.46
PSW-Poly	152	108	177	152	11.40	132	166	152	4.62	151	156	153	1.20	110	179	151	12.12
SD-Poly	502	464	523	501	10.89	446	507	489	10.47	481	514	503	5.64	427	525	485	17.00
(b) Magnitude Only																	
		Min	*Max*	*Mean*	σ	*Min*	*Max*	*Mean*	σ	*Min*	*Max*	*Mean*	σ	*Min*	*Max*	*Mean*	σ
PSW-3D	99	98	101	99	0.56	99	99	99	0.00	99	99	99	0.00	95	98	96	0.56
SD-3D	556	555	557	556	0.66	553	556	555	0.58	550	564	556	2.59	563	567	566	0.88
PSW-Poly	152	152	154	153	0.60	152	153	152	0.17	152	153	152	0.50	151	154	152	0.61
SD-Poly	502	497	510	504	2.80	503	507	504	0.89	501	507	504	1.01	497	512	506	3.04
(c) Direction Only																	
		Min	*Max*	*Mean*	σ	*Min*	*Max*	*Mean*	σ	*Min*	*Max*	*Mean*	σ	*Min*	*Max*	*Mean*	σ
PSW-3D	99	93	110	100	3.32	94	106	99	1.91	99	99	99	0.00	85	110	97	3.75
SD-3D	556	549	564	557	2.45	548	572	555	3.53	525	564	554	9.86	557	585	567	4.23
PSW-Poly	152	117	184	154	10.20	121	160	151	5.77	151	157	153	1.10	117	189	152	11.22
SD-Poly	502	468	529	501	10.67	441	506	488	11.70	491	515	501	5.23	447	522	484	14.63